Regulating the metal-insulator transition of *RE*$BaCo_2O_{5+\delta}$ combining *RE*-substitution and anion control

Fang Zhang[1†], Yuchen Cui[2†], Jingxin Gao[2], Hao Zhang[2], Yi Bian[2], Chen Liu[3], Nuofu Chen[1*], and Jikun Chen[2*]

[1]School of Renewable Energy, North China Electric Power University, Beijing 102206, China
[2]School of Materials Science and Engineering, University of Science and Technology Beijing, Beijing 100083, China
[3]Beijing Synchrotron Radiation Facility, Institute of High Energy Physics, Chinese Academy of Sciences, Beijing 100049, China

[†]F. Zhang and Y. Cui contribute equally
*Correspondence: Nuofu Chen (nfchen@ncepu.edu.cn) and Jikun Chen (jikunchen@ustb.edu.cn)

Table S1 Details for the sample synthesis and refinement of as-synthesized *RE*$BaCo_2O_{5+\delta}$ in air, refined using the *Pmmm* space group

RE	*Space group*	2*a*, Å	*b*, Å	*c*, Å	*V*, (Å)^3	R_p	R_{wp}	R_{exp}	χ^2
Pr	*Pmmm*	7.807	7.817	7.630	232.849	4.86	6.29	4.65	1.83
Nd	*Pmmm*	7.796	7.809	7.612	231.736	6.33	8.34	4.21	3.91
Sm	*Pmmm*	7.778	7.846	7.551	230.457	6.49	8.58	4.38	3.84
Eu	*Pmmm*	7.783	7.824	7.535	229.464	6.95	9.29	6.61	1.97
Gd	*Pmmm*	7.776	7.818	7.524	228.735	6.46	9.04	6.12	2.18
Tb	*Pmmm*	7.737	7.816	7.514	227.264	5.46	7.02	5.66	1.54
Dy	*Pmmm*	7.762	7.782	7.499	226.516	4.85	6.89	3.86	3.19
Ho	*Pmmm*	7.747	7.752	7.496	225.091	5.33	7.07	4.28	2.73

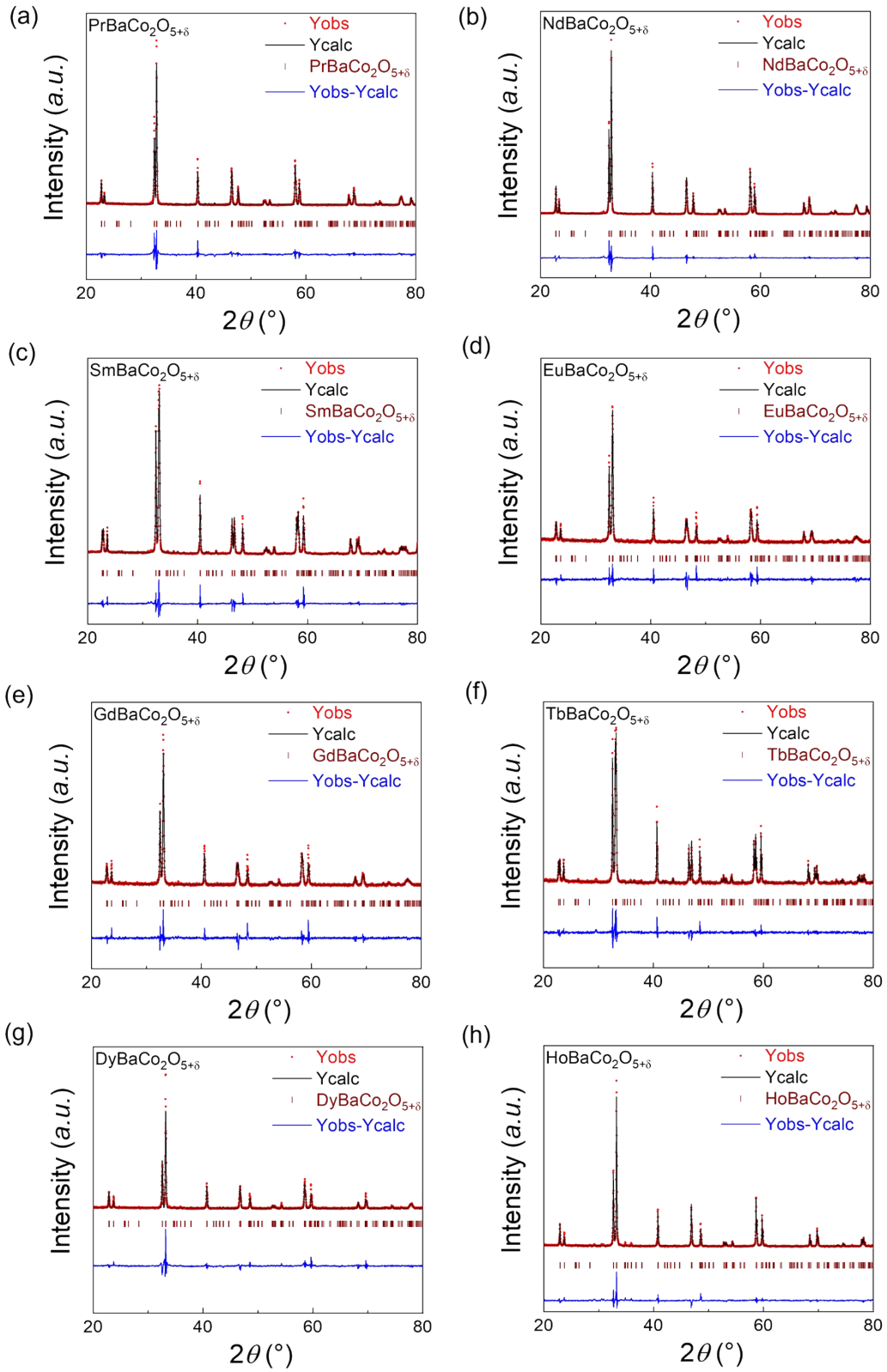

Fig. S1 The X-ray diffraction (XRD) patterns and refinements for as-synthesized *RE*$BaCo_2O_{5+\delta}$. (a)-(h) corresponds to samples No.1-No.8 listed in Table S1, respectively.

Table S2 Details for the sample synthesis and refinement of as-synthesized *RE*$BaCo_2O_{5+\delta}$ in air, refined using the *P4/mmm* space group

RE	*Space group*	2*a*, Å	*b*, Å	*c*, Å	*V*, (Å)^3	R_p	R_{wp}	R_{exp}	χ^2
Pr	*P4/mmm*	7.812	—	7.630	116.418	6.67	9.43	4.65	4.11
Nd	*P4/mmm*	7.803	—	7.612	115.883	6.16	8.49	4.21	4.08
Dy	*P4/mmm*	7.771	—	7.501	113.252	5.88	8.54	4.13	4.28
Ho	*P4/mmm*	7.753	—	7.499	112.694	4.58	5.91	4.27	1.91

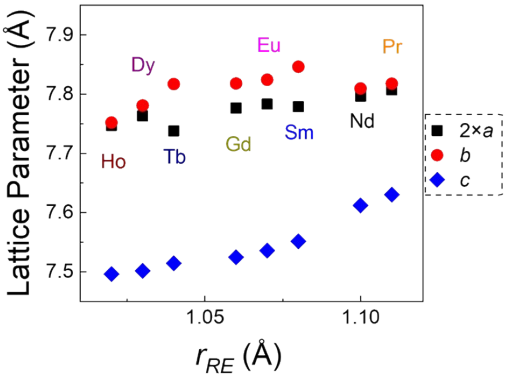

Fig. S2 The lattice parameters for as-synthesized *RE*$BaCo_2O_{5+\delta}$ in air plotted as a function of the ionic radius of rare-earth, refined using the *Pmmm* space group

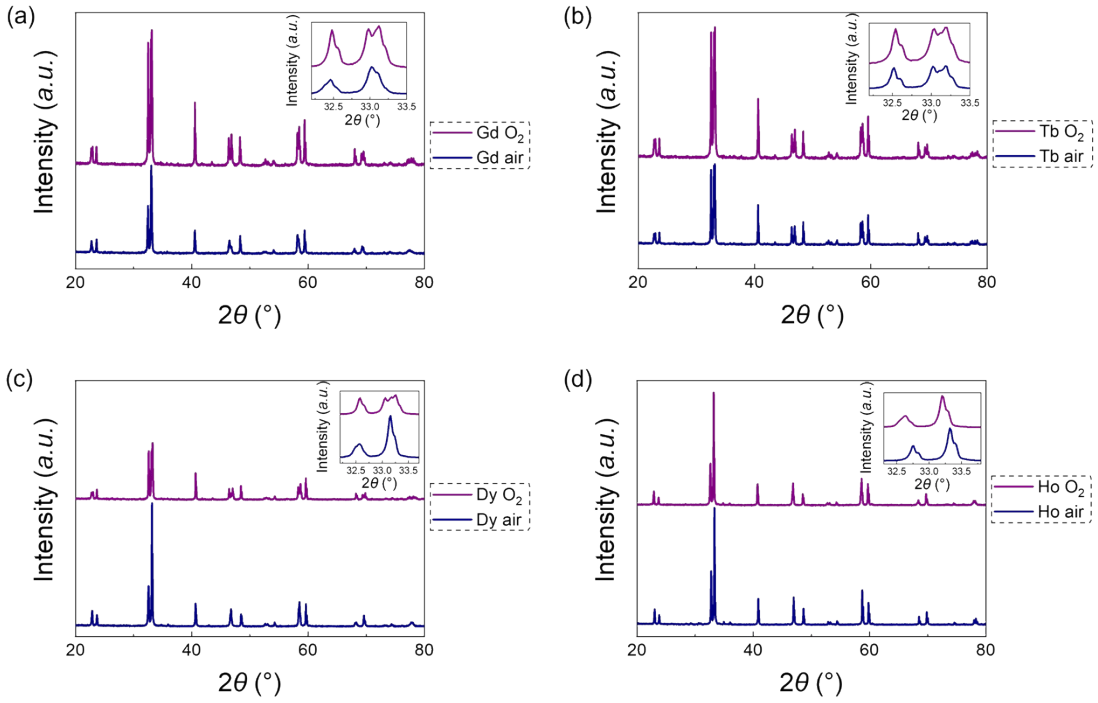

Fig. S3 The X-ray diffraction (XRD) patterns for *RE*$BaCo_2O_{5+\delta}$ synthesized in air and annealed in Mpa-high oxygen. (a)-(d) corresponds to $GdBaCo_2O_{5+\delta}$, $TbBaCo_2O_{5+\delta}$, $DyBaCo_2O_{5+\delta}$ and $HoBaCo_2O_{5+\delta}$, respectively.

Table S3 Details for the sample synthesis and refinement of *RE*$BaCo_2O_{5+\delta}$ annealed in 5 Mpa oxygen for 24 hours at 300 °C

RE	*Space group*	2*a*, Å	*b*, Å	*c*, Å	*V*, (Å)^3	R_p	R_{wp}	R_{exp}	χ^2
Gd	*Pmmm*	7.750	7.823	7.531	228.340	5.14	7.34	4.05	3.29
Tb	*Pmmm*	7.734	7.813	7.518	227.191	5.45	7.87	3.90	4.07
Dy	*Pmmm*	7.722	7.810	7.506	226.371	5.30	7.85	3.97	3.92

Ho	*Pmmm*	7.746	7.765	7.491	225.353	6.07	8.87	3.92	5.11

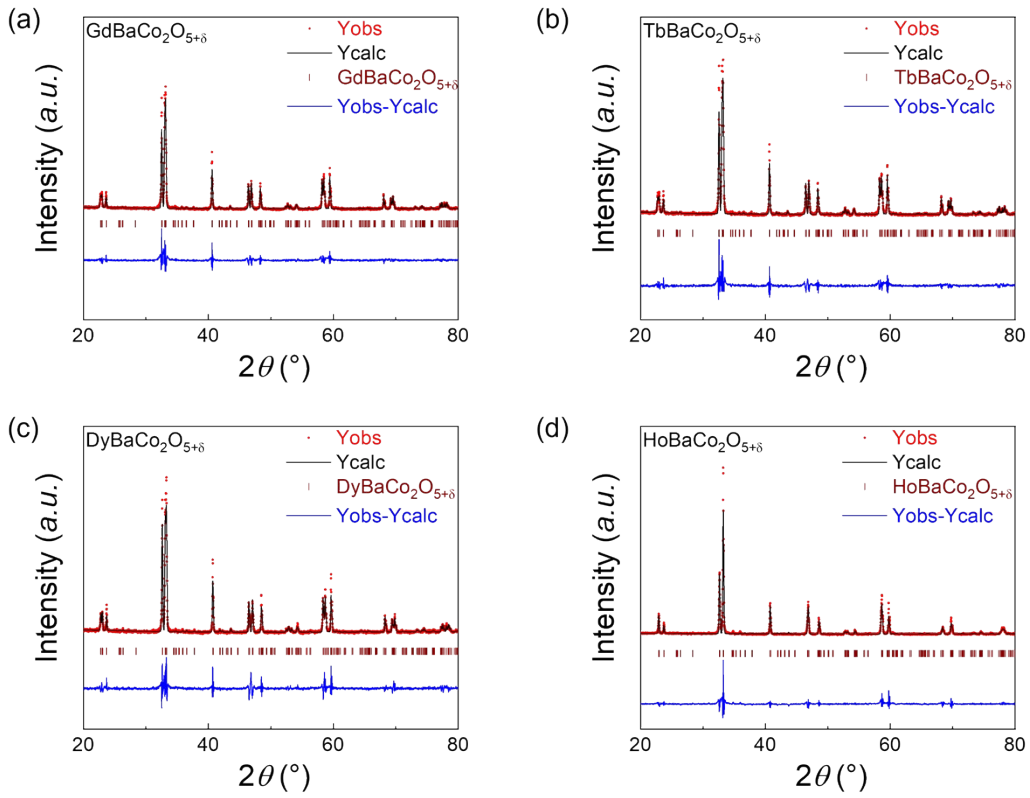

Fig. S4 The X-ray diffraction (XRD) patterns and refinements for *RE*$BaCo_2O_{5+\delta}$ annealed in Mpa-high oxygen. (a)-(d) corresponds to samples No.1-No.4 listed in Table S3, respectively.

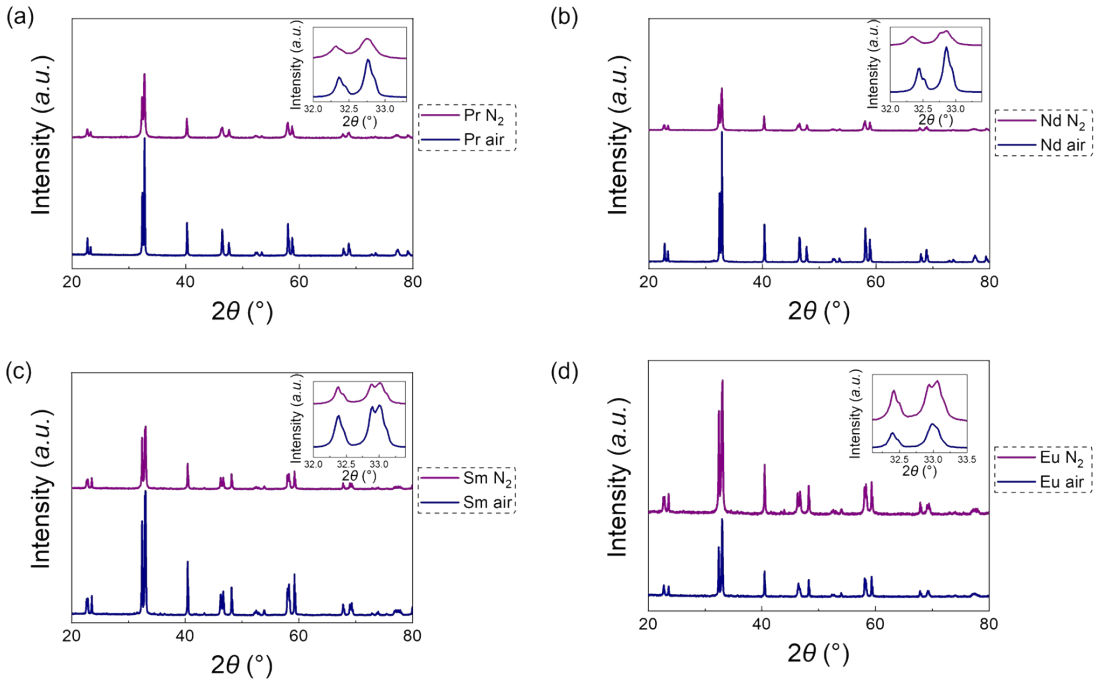

Fig. S5 The X-ray diffraction (XRD) patterns for *RE*$BaCo_2O_{5+\delta}$ synthesized in air and annealed in N_2 flow. (a)-(d) corresponds to $PrBaCo_2O_{5+\delta}$, $NdBaCo_2O_{5+\delta}$, $SmBaCo_2O_{5+\delta}$ and $EuBaCo_2O_{5+\delta}$, respectively.

Table S4 Details for the sample synthesis and refinement of *RE*$BaCo_2O_{5+\delta}$ annealed in nitrogen for 12 hours at 300 °C

RE	*Space group*	2*a*, Å	*b*, Å	*c*, Å	*V*, (Å)^3	R_p	R_{wp}	R_{exp}	χ^2
Pr	*Pmmm*	7.804	7.851	7.630	233.818	6.84	9.59	4.51	4.52
Nd	*Pmmm*	7.794	7.851	7.600	232.585	6.45	8.93	4.30	4.31
Sm	*Pmmm*	7.775	7.847	7.552	230.391	6.60	9.41	4.43	4.51
Eu	*Pmmm*	7.764	7.835	7.538	229.342	5.95	8.43	4.20	4.03

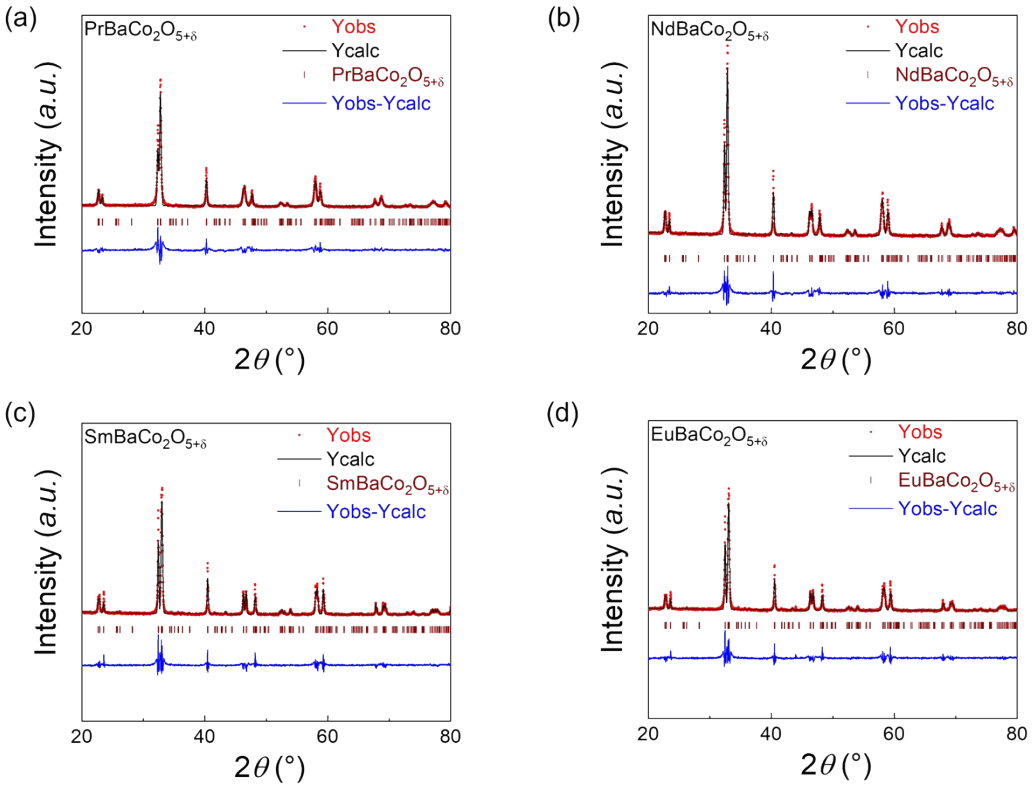

Fig. S6 The X-ray diffraction (XRD) patterns and refinements for *RE*$BaCo_2O_{5+\delta}$ annealed in N_2 flow. (a)-(d) corresponds to samples No.1-No.4 listed in Table S4,

respectively.

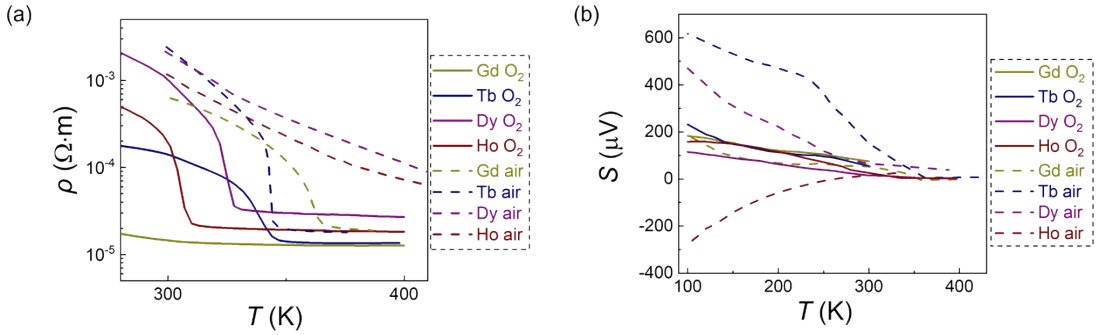

Fig. S7 (a) The relationship between resistivity and temperature for high-pressure oxygen-annealed and air-synthesized *RE*$BaCo_2O_{5+\delta}$. (b) The relationship between seebeck coefficient and temperature for high-pressure oxygen-annealed and air-synthesized *RE*$BaCo_2O_{5+\delta}$.

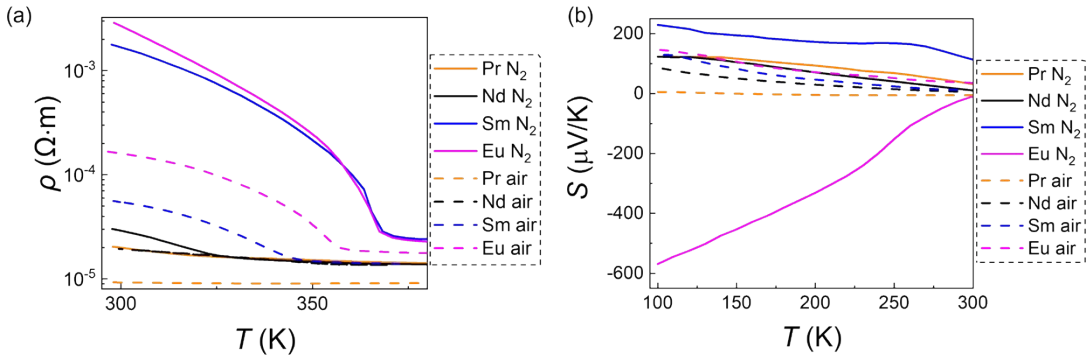

Fig. S8 (a) The relationship between resistivity and temperature for nitrogen - annealed and air-synthesized *RE*$BaCo_2O_{5+\delta}$. (b) The relationship between seebeck coefficient and temperature for nitrogen-annealed and air-synthesized *RE*$BaCo_2O_{5+\delta}$.

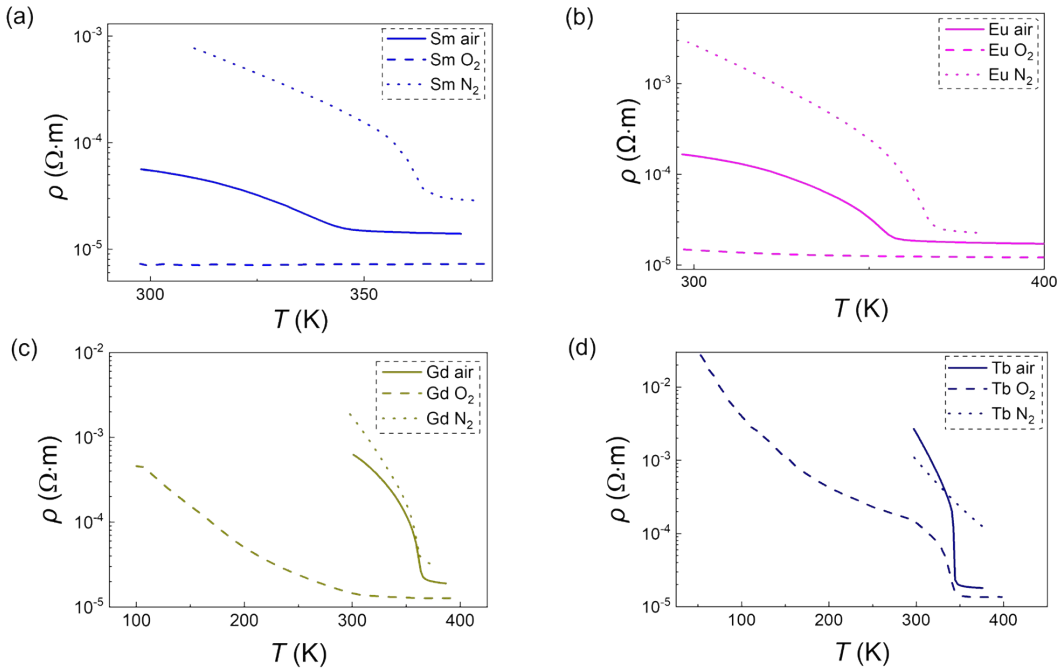

Fig. S9 Resistivity as a function of temperature for high-pressure oxygen-annealed, nitrogen-annealed and air-synthesized REBaCo$_2$O$_{5+\delta}$. (a)-(d) corresponds to SmBaCo$_2$O$_{5+\delta}$, EuBaCo$_2$O$_{5+\delta}$, GdBaCo$_2$O$_{5+\delta}$ and TbBaCo$_2$O$_{5+\delta}$, respectively.

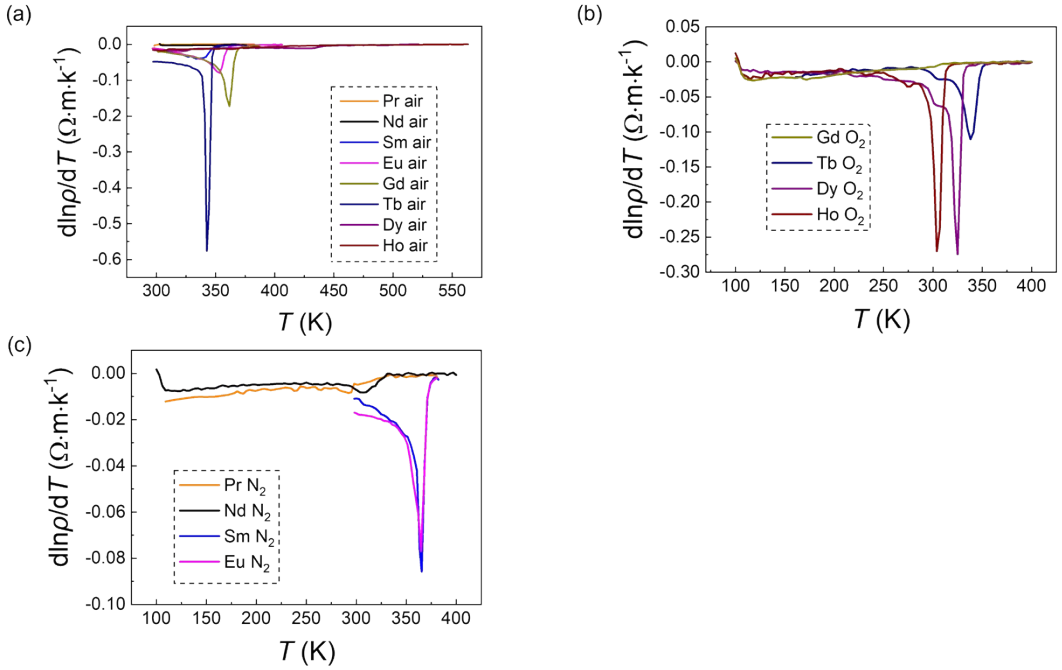

Fig. S10 (a) d(lnρ)/d(T)-T tendency for REBaCo$_2$O$_{5+\delta}$ (RE= Pr, Nd, Sm, Eu, Gd, Tb, Dy, Ho) polycrystalline ceramic samples synthesized in the air, and the temperature of the peak is defined as T_{MIT}. (b) d(lnρ)/d(T)-T tendency for REBaCo$_2$O$_{5+\delta}$ (RE= Gd, Tb, Dy and Ho) polycrystalline ceramic samples annealed in Mpa-high oxygen, and the temperature of the peak is defined as T_{MIT}. (c) d(lnρ)/d(T)-T tendency for REBaCo$_2$O$_{5+\delta}$ (RE= Pr, Nd, Sm and Eu) polycrystalline ceramic samples annealed in N_2 flow, and the temperature of the peak is defined as T_{MIT}.

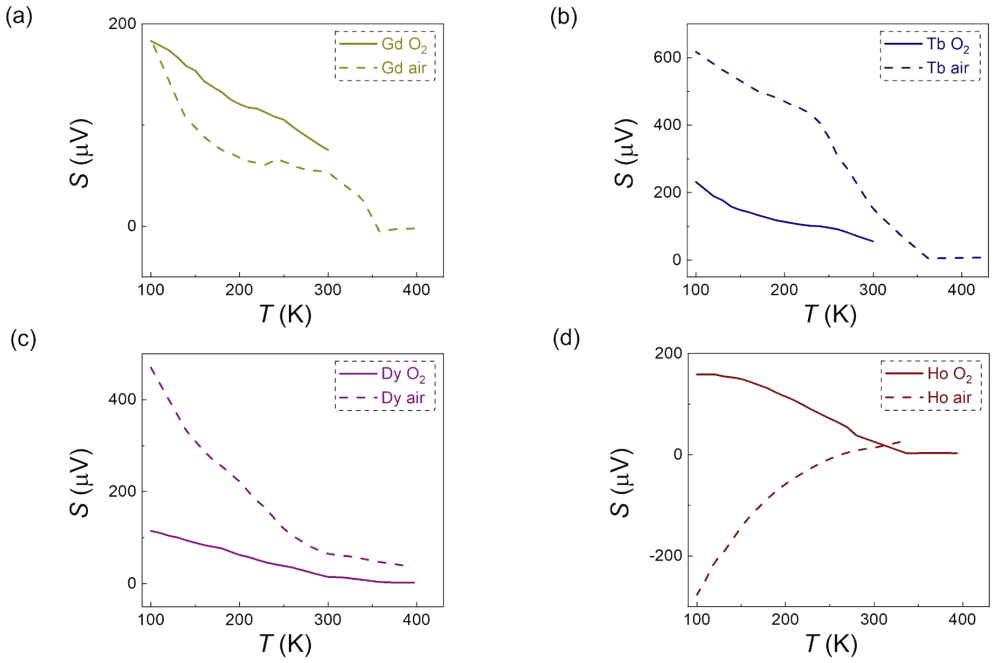

Fig. S11 Comparison of the Seebeck coefficient as a function of temperature for *RE*$BaCo_2O_{5+\delta}$ synthesized in air and post-annealed in high pressure oxygen. (a), $GdBaCo_2O_{5+\delta}$. (b), $TbBaCo_2O_{5+\delta}$. (c), $DyBaCo_2O_{5+\delta}$. (d), $HoBaCo_2O_{5+\delta}$. The post-annealing process alters the δ away from 0.5, as evidenced by a reduction in the absolute value of the Seebeck coefficient for all samples, consistent with the previous reports[1]. It is worth noticing that the $HoBaCo_2O_{5+\delta}$ exhibits the most significant change (e.g., the Seebeck coefficient switching from negative to positive), indicating a change in the dominant carrier type.

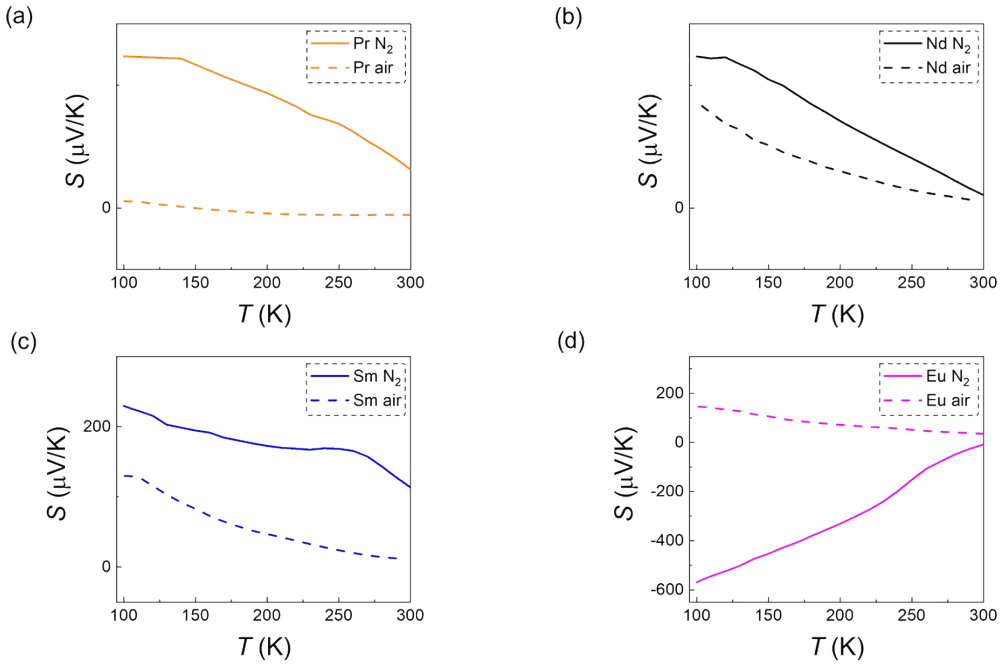

Fig. S12 Comparison of the Seebeck coefficient as a function of temperature for *RE*$BaCo_2O_{5+\delta}$ synthesized in air and post-annealed in nitrogen. (a), $PrBaCo_2O_{5+\delta}$. (b), $NdBaCo_2O_{5+\delta}$. (c), $SmBaCo_2O_{5+\delta}$. (d), $EuBaCo_2O_{5+\delta}$. In contrast to the oxygen-annealed samples as shown in Fig. S11, the absolute Seebeck coefficient increases for all samples after nitrogen annealing, indicating that δ shifts closer to 0.5 after nitrogen treatment. It is worth noticing that the $EuBaCo_2O_{5+\delta}$ exhibits the most significant change (e.g., the Seebeck coefficient switching from negative to positive), demonstrating a reversal of the dominant carrier type.

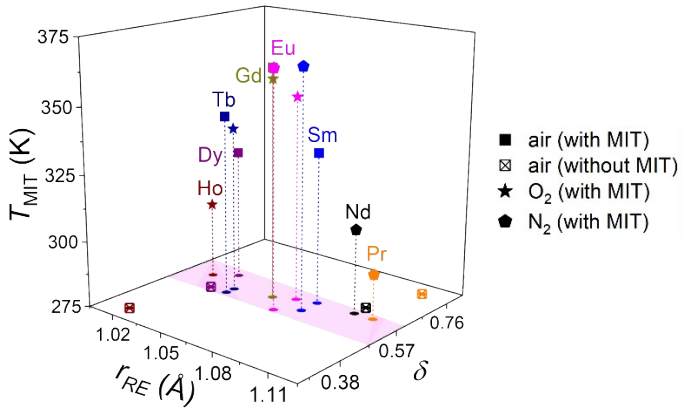

Fig. S13 The metal-insulator transition temperature (T_{MIT}) plotted as a function of

rare-earth ionic radius(r_{RE}) and oxygen content.

It can be observed that metal-insulator transition temperature (T_{MIT}) of *Re*$BaCo_2O_{5+\delta}$ exhibits a non-monotonic dependence on the rare-earth ionic radius (r_{RE}), indicating the regulation of rare-earth composition on T_{MIT}. It is also worth noticing that the metal-insulator transition (MIT) behavior of *Re*$BaCo_2O_{5+\delta}$ is observed only when δ is close to 0.5. This is because deviations from this stoichiometry reduce the Co^{3+} concentration, thereby suppressing MIT, which is associated with the spin-state of Co^{3+} ions, consistent with the previous reports[1]. These observations demonstrate that both structural symmetry and the concentration of Co^{3+} ions are critical factors in stabilizing MIT in *Re*$BaCo_2O_{5+\delta}$.

1. A. A. Taskin, et al., Transport and magnetic properties of $GdBaCo_2O_{5+x}$ single crystals: A cobalt oxide with square-lattice CoO_2 planes over a wide range of electron and hole doping, *Phys. Rev. B*, 2005, **71,** 134414.